Developing an optical fiber biosensor for the detection of CD44 protein with breast cancer cells

Medina Shuriyeva, Bachelors in Biological Sciences

Submitted in fulfilment of the requirements for the degree of Master of Science in Biomedical Engineering

School of Engineering and Digital Sciences
Department of Chemical and Materials Engineering
Nazarbayev University

53 Kabanbay Batyr Avenue,
Astana, Kazakhstan, 010000

Supervisor: Daniele Tosi
Co-Supervisor: Cevat Erisken

Date: 11.04.2025

DECLARATION

I hereby, declare that this manuscript, entitled “Developing an optical fiber biosensor for the detection of CD44 protein with breast cancer cells”, is the result of my own work except for quotations and citations which have been duly acknowledged.

I also declare that, to the best of my knowledge and belief, it has not been previously or concurrently submitted, in whole or in part, for any other degree or diploma at Nazarbayev University or any other national or international institution.

Name: Medina Shuriyeva

Date: 11.04.2025

Table of Contents

Abstract

CD44, the transmembrane glycoprotein functions as a cancer stem cell biomarker, as it supports cell attachment as well as cell movements, leading to tumor cell progression. The excessive overexpression of CD44 is strongly associated with unfavorable cancer progression and metastasis in several cancer types such as breast cancer. Existing detection methods for CD44 such as ELISA and immunohistochemistry together with Western blotting face limitations in both processing complexity and time requirements. Additionally, they are limited in terms of sensitivity. Optical fiber biosensors provide researchers with a sensitive method that performs real-time label-free measurements. This thesis project describes and discusses the fabrication, calibration, and detection processes of a novel optical fiber biosensor which detects CD44 through commercially sourced cell lines. The sensor worked with anti-CD44 antibodies at its surface while testing sucrose-based refractive index standards which yielded 125.23 dB/RIU sensitivity. A sensor detection procedure used three human cell lines: HCC1806 with CD44 expression and MCF10A without it as well as HEK293 with no CD44 expression. The sensor demonstrated high sensitivity to HCC1806 cells through a distinct intensity decrease at 1544.416 nm (3.315 dB) but revealed minimal detection of MCF10A cells (0.110 dB) thus proving its specific detection capabilities. Research progressed to evaluate non-specific interactions after HEK293 cells produced signal magnitude of 2.289 dB. The sensor system proved its capability to function as a specific tool for quick detection of CD44-expressing cells thereby opening prospects for future cancer screening and metastasis monitoring.

Acknowledgements

I would like to express my gratitude to the individuals who have supported me throughout my thesis work and contributed to the completion of this project. First of all, I would like to thank my lead supervisor, Professor Daniele Tosi, for his support and gentle supervision, as well as his awareness of the importance of creating a non-toxic atmosphere within the laboratory environment. I would also like to express my gratitude to my co-supervisor, Professor Cevat Erisken, for his assistance within this thesis project, and outside the scope of the thesis work, including his academic supervision as a program director and the course instructor.

There are laboratory team members who have significantly helped me during my unexpected transfer to the new lab and a new project. I personally want to thank Marzhan, Aida, Aliya Bekmurzayeva, Aidana, Kanagat, Kuanysh, Maham, and Zhandos for their willingness to assist and train me.

Finally, I would like to thank my mother Zhannat, my sister Amina, and my dearest friends Ainel, Aruzhan, and Kamilla for their patience and support during this challenging academic year. Without these individuals, I would not have been able to finish even 10% of the thesis work.

List of abbreviations

CD44	Cluster of Differentiation
DCIS	Ductal Carcinoma In Situ
IDC	Invasive Ductal Carcinoma
ILC	Invasive Lobular Carcinoma
FOXA2	Forkhead Box Protein A2
WBA	Western Blot Analysis
ELISA	Enzyme-Linked Immunosorbent Assay
SMF	Single-Mode Fiber
SEM	Scanning Electron Microscopy
OFS	Optical fiber sensor
SMF	Single-Mode Fiber
RI	Refractive Index
NIR	Near-red region
RIU	Refractive Index Units
APTMS	(3-Aminopropyl)trimethoxysilane
GA	Glutaraldehyde
PBS	Phosphate-buffered Saline

m-PEG amine	methoxy-polyethylene glycol amine
HEK293	Human Embryonic Kidney 293 cells
MCF10A	Michigan Cancer Foundation 10A cells
HCC1806	Human Breast Carcinoma cell line 1806
IREC	Institutional Research Ethics Committee
DMEM	Dulbecco's Modified Eagle Medium

CHAPTER 1 - INTRODUCTION

1.1 CDD 44

Cluster of differentiation 44 (CD44) is a complex adhesion transmembrane glycoprotein, the normal function of which is associated with cellular aggregation and migration, activation of lymphocytes, development of new blood vessels, cytokine release, and many more [1,2]. Its overexpression, however, signals about the development of tumors, acting as a biomarker of the expression of cancer stem cells [3]. Ziranu et al., for example, in their research, showed a high association between great expression of CD44 and metastatic colorectal cancer after conducting statistical analysis collected from 2009 to 2021 [4]. In their study, they also identified that there was a high correlation between CD44 overexpression and poorer prognosis, as well as chemotherapy resistance among 65 patients found with metastatic colorectal cancer. Another study suggests that an increased CD44 expression is related to such cancer types as low-grade glioma, mesothelioma, and pancreatic adenocarcinoma [5].

1.2 Breast Cancer

Breast cancer remains the main cause of women's deaths related to cancerous diseases [6]. Only in 2020, it was estimated to have reported 2.3 million new breast cancer cases with almost 700,000 deaths [7]. Ductal carcinoma in situ (DCIS) is the most prevalent type of pre-invasive breast cancer, having only 10%–30% of cases proceeding to invasive cancer, and the prediction of biomarkers for the development of invasive or metastatic disease is not as effective as is required [6]. A diverse range of conditions known as invasive carcinomas are further classified based on the morphology of the cells. The most frequent type of invasive carcinoma is invasive ductal carcinoma (IDC), accounting for 60%–75% of cases, and

invasive lobular carcinoma (ILC), which accounts for 10%–15% of tumors [6]. It has been reported that CD44 protein is highly associated with breast cancer cells and its overexpression can be found in breast cancer metastases [8]. Moreover, in research conducted by Vadhan et al., the expression of CD44 protein was studied via flow cytometry in tissue samples obtained from 14 breast cancer patients [9]. It was identified that CD44 expression had been higher in metastatic lymph nodes compared to primary tumors as can also be seen in *Figure 1* .

Figure 1. Flow cytometric analysis of CD44 expression in primary breast tumors (T) and paired metastatic lymph nodes (LN) in 14 breast cancer patients' samples. (Vadhan et al., 2022)

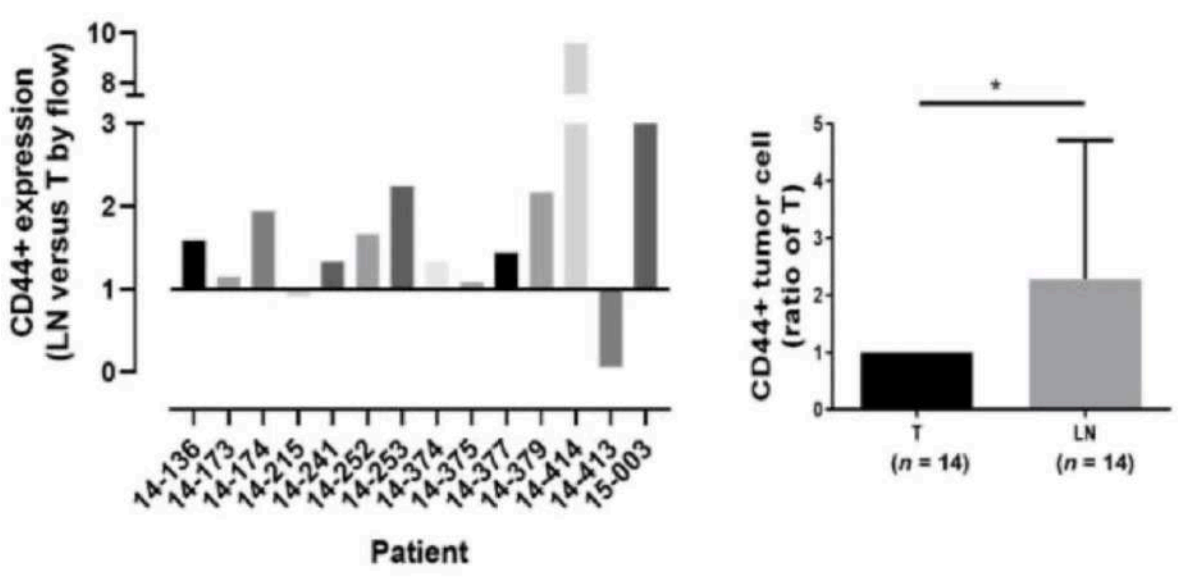

As shown in Figure 1, there is a significant difference between the expression of CD44 in lymph nodes compared to the primary tumor cells, suggesting that CD44 is predominantly produced in tissues invaded by cancer stem cells. Another important finding to mention within their research is the correlation between CD44 and the invasion of breast cancer cells. By controlling the localization of Forkhead box protein A2 (FOXA2), phosphorylation of AKT pathway takes place, leading to the reduction of E-Cadherin synthesis, hence enhancing

cancer migration and invasion. This suggests that using CD44 as a biomarker of cancer stem cells can also improve the therapeutic effect by knocking down its overexpression. Additionally, its detection during the primary stages of tumor metastasis can increase the chance of survival and make the treatment more effective [9].

1.3 State-of-art and Problem Statement

Currently, there are several ways assays designed for CD44 protein detection. The main methods include immunochemistry, WBA (Western blot analysis), and ELISA (enzyme-linked immunosorbent assay) [10]. Bekmurzayeva et al., in her research, shared a list of several CD44 detecting assays available in the market, including Commercial ELISA kits, Sandwich ELISA, Fluorescence resonance energy, Solid-phase proximity ligation assay, electrochemical, and photoelectrochemical assays, ball resonators [10]. Another assay available in the market is the lateral flow assay that proceeds CD44 detection on saliva [11]. However, these methods are time-consuming and are characterized as not sensitive and specific [10]. Biosensors, in contrast, offer a promising solution, being more time-efficient and sensitive to the environment [12]. Biosensors based on optical fibers are reported to be effective in terms of biochemical reactions, reaction kinetics, fast chemical detection, and a potential for remote control [13]. Bekmurzayeva et al. have previously developed an optical fiber biosensor for CD44 detection using a ball resonator [10]. They were able to design a sensitive and specific biosensor based on a single-mode fiber (SMF) and tested the sensor under dynamic conditions mimicking blood flow. One of their limitations included a low scattering range, leading to a lower detection spectrum. Thus, it is proposed to introduce optical fiber doped with nanoparticles, namely, MgO that have previously been reported as a method to work with biosensors on a greater scattering range [14]. As CD44 protein detection

is essential for cancer detection during metastatic tumor development, it is crucial to design a device that will be able to detect the protein in a limited amount of time, being biocompatible and inexpensive. Biosensor based on an optical fiber doped with nanoparticles has a promising potential on this matter. This thesis project aimed at fabricating, optimizing, and functionalizing optical fiber for its consequent cell detection.

CHAPTER 2 – MATERIALS AND METHODS

2.1. Fabrication and calibration of the sensors

The fabrication process consists of two main steps - cleaving the fibers and splicing them to each other. All optical fiber sensors were fabricated by a fusion of an (simple-distributed interferometer) SDI fiber and an SMF, spliced by Fujikura 36S laser splicing machine. To successfully splice the fibers with each other and reach a desired sensitivity, each of the fibres were first cut by a Tumtec A9 cleaver, shown in *Image 1*.

Image 1. A demonstration of SMF ready to be cleaved and cut by the cleaver

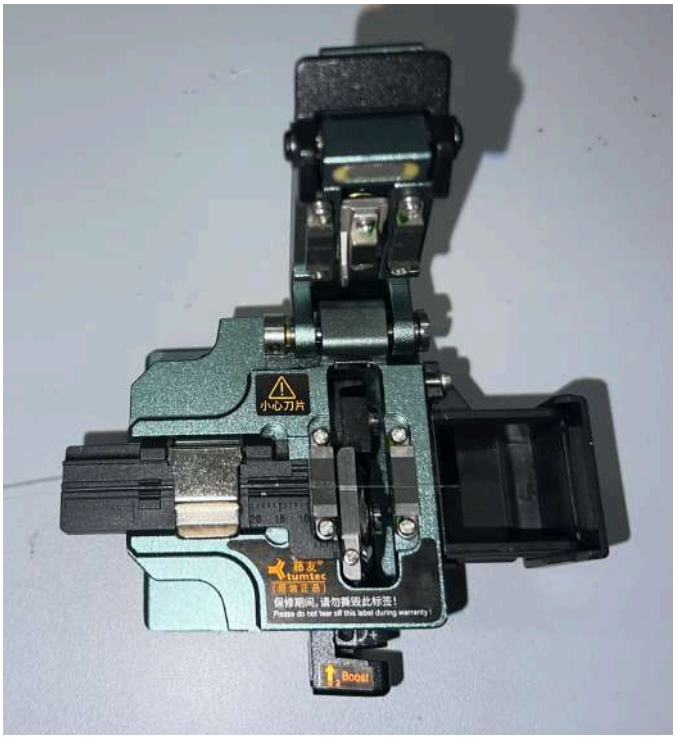

The Fujikura 36s uses a heat laser to fuse the splicers together [14]. *Image 2* demonstrates the process of splicing the two fibres with each other.

Image 2. The fusion process of the two fibers by Fujikura 36s

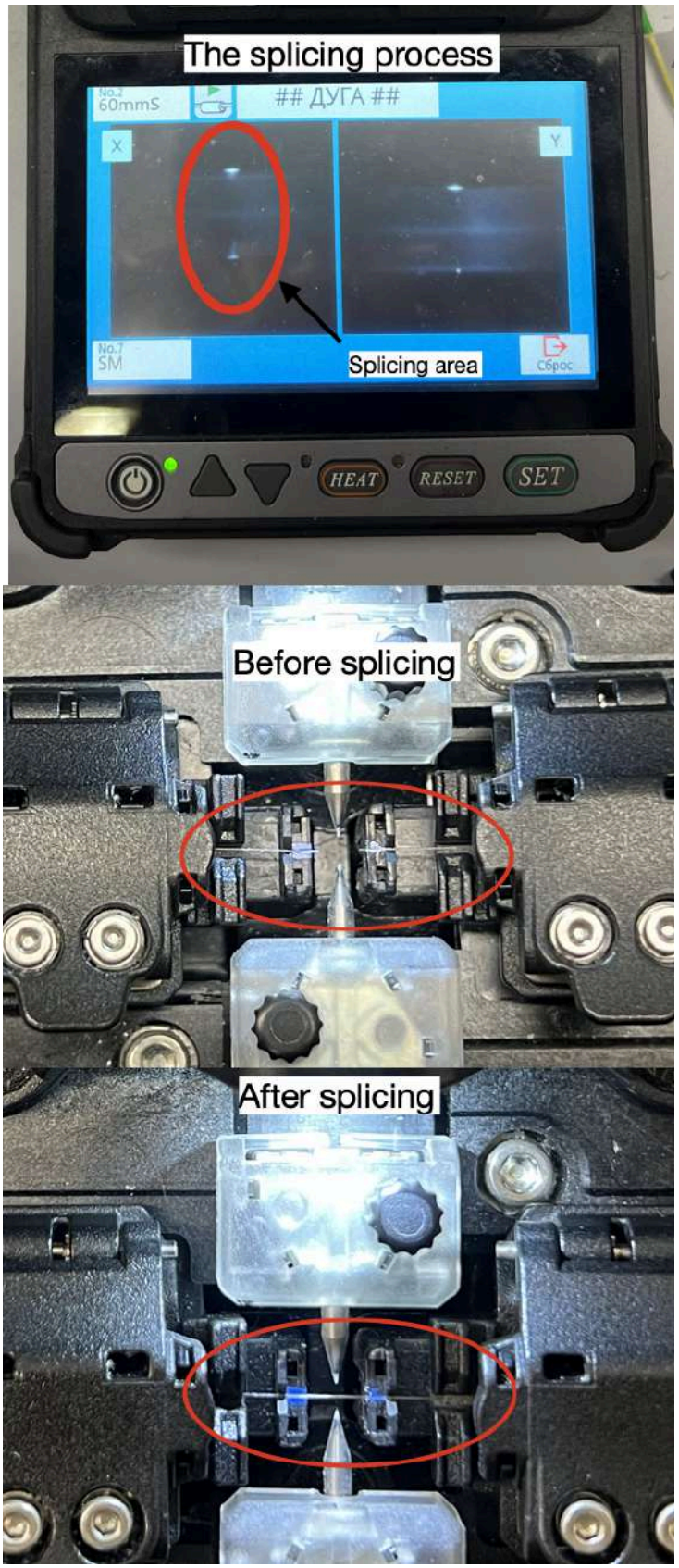

After the fibers were fabricated, they were calibrated by classic Refractive Index (RI) Calibration technique in a sucrose solution since it has well-defined optical properties.

Sucrose solutions provide a precise and reproducible tuning of refractive index values across a biologically relevant range, mimicking the optical environment of protein solutions, serum, and cell suspensions [15]. Additionally, they exhibit minimal absorption in the near-infrared (NIR) region, making it a convenient tool for calibration of fiber optic biosensors that operate in the 1300–1600 nm spectral window. Since they are convenient to prepare, comparably cheap, and chemically stable, sucrose solutions are widely used for RI measurements [15]. The channels of the Micron Optics si255 industrial sensing interrogator were connected to the fibers. The fiber tips were introduced to the 6mL of 10% of sucrose solution in a falcon tube cap. A sensing analyzing software ENLIGHT was used to save the data in a .txt format. Three files per RI were saved to have more reliable results. Overall, 6 RI's were measured with consequent addition of 400 uL of 40% of the sucrose solution. *Image 3* demonstrates the calibration setup. All measurements were then analyzed using MATLAB software, the process of which is discussed in the next section.. Refractive index changes sensitivity was assessed using sucrose calibration solutions at the refractive index units (RIU) values of 1.34761 ~ 1.35845. The resonance wavelengths associated with each spectral feature (peak or valley) were tracked across the RI series for each spectral feature. The most appropriate sensor type is determined by applying a linear regression to the plot of wavelength against refractive index and defining the slope of the fit (in nm/RIU) as the sensor's sensitivity. The rounding took place only if the coefficient of determination for the feature was greater. Highly reflective sensors of sensitivity of 100 nm/RIU and higher were proceeded to the functionalization step.

Image 3. A calibration setup

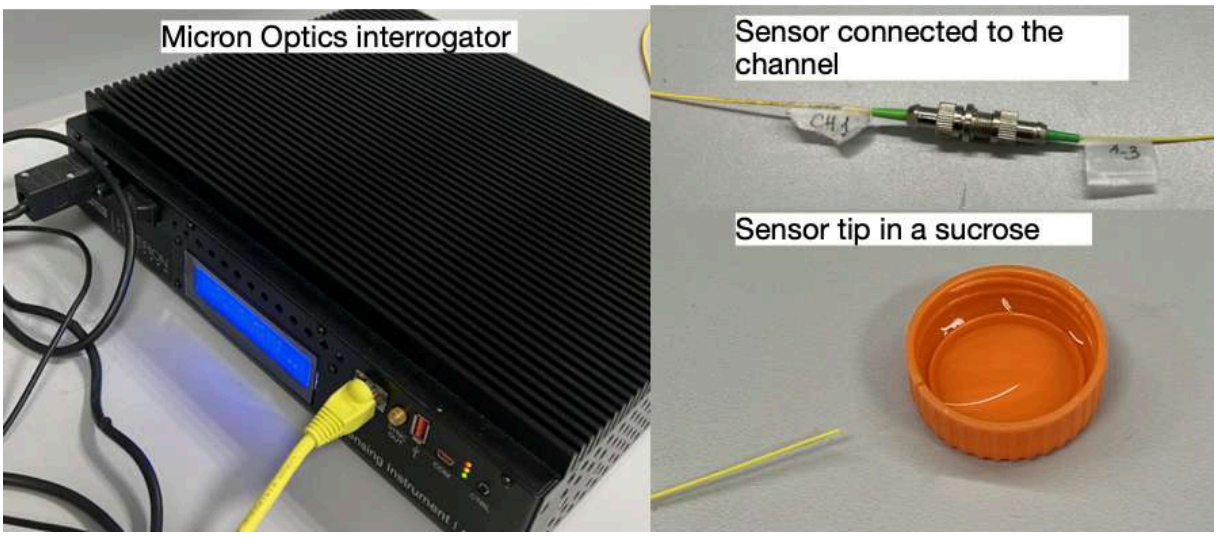

2.2 Functionalization

To ensure the successful attachment of CD44 antibodies on the tip of the fiber, the fibers were treated with several solutions and procedures. The sensor functionalization process followed pre-established methods with some adjustments [16]. The first steps included suspending the SDI in piranha solution to clean out the surface of the sensors them for 15 minutes with a ratio of 4:1 of sulfuric acid (H_2SO_4) and hydrogen peroxide (H_2O_2). The treatment had two main functions: it removed organic residues and provided hydroxyl groups availability on the surface tip of the sensor. Both factors enhance the fiber's potential for subsequent chemical modification. The fibers received distilled water washing after which they were dried with a nitrogen stream. The sensors were exposed to a 20-minute immersion in (3-aminopropyl)trimethoxysilane (APTMS) methanol solution at 1% concentration to develop amine groups. Following that, the sensors were additionally rinsed by methanol. To improve the stabilization conditions of he sensor surface, the next step required heating them to 110 °C for one hour following. A solution containing 25% glutaraldehyde (GA) in

phosphate-buffered saline (PBS) was used to incubate the fibers for one hour while creating reaction sites for biomolecule binding. The sensors then received several PBS washes before being exposed to 4 μg/mL monoclonal anti-CD44 antibody for one hour under continuous gentle rinsing to reach a thorough distribution of the antibodies.. Nonspecific adsorption was minimized through the blocking procedure that used a 1% solution of methoxy-polyethylene glycol amine (mPEG-amine) which treated the fibers for 30 minutes. The functionalized sensors received a washing solution of PBS before they were kept for storage at 4 °C. The researchers used this exact preparation method to make sensors intended for specificity testing.

2.3 Cell culture and detection

In this study, the three different commercial human cell lines were used: HCC1806 (epithelial breast cancer), HEK293 (human embryonic kidney) and MCF10A (non tumorigenic breast epithelial). Because the cell lines used are commercially available, there was no need in the Research Ethics Committee (IREC) permission. Cells were cultured according to each cell line's specific requirements. RPMI-1640 medium supplemented with 10% fetal bovine serum (FBS) and grown at 37 °C in humidified atmosphere of 5% CO_2 were used to grow HCC1806 cells. The same incubation conditions were used to culture HEK293 cells in Dulbecco's Modified Eagle Medium (DMEM) with 10% FBS and 1% penicillin-streptomycin. DMEM/F12 medium containing 5% horse serum, 20 ng/mL epidermal growth factor (EGF), 0.5 μg/mL hydrocortisone, 100 ng/mL cholera toxin, 10 μg/mL insulin, and 1% penicillin-streptomycin was used to maintain MCF10A cells. All cell lines were harvested at between 80 and 90% confluency. Accutase™, used to avoid enzymatically digesting the cells, was used to detach HCC1806 cells, while HEK293 and MCF10A cells were dissociated with 0.05% trypsin-EDTA. Cells were incubated at 37 °C for

5–8 min and then neutralized by fresh medium. Cell suspensions were centrifuged at 125–200 × g for 5 minutes, resuspended in PBS and passed through a 40 μm cell strainer to achieve uniform single cell suspension. The trypan blue exclusion method was used to test for cell viability and determination of concentration performed by hemocytometer. PBS serial dilutions were prepared from 1×10^6 to 1 cell/mL lowest for usage in the detection experiments. *Table 1* displays applied concentrations and cell dilutions to all three types of cell lines. The cell suspension was centrifuged at 125 ×g for 5 minutes enriched with the cells. After the pellet, the suspension was resuspended in PBS and the suspension passed through a 40 μm cell strainer generating a fermented uniform single pellet cell product. A stock solution was made and serially diluted in PBS from 1×10^6 cells/mL to 1 cell/mL. The functionalized optical sensors were then incubated with a solution of the same concentration.

Table 1. Serial dilution scheme used for sensor detection experiments.

Concentration Index	**Cell Count**	**Description**
1	0	PBS only
2	1	Single-cell detection
3	10	10^1 cells/mL
4	100	10^2 cells/mL
5	1000	10^3 cells/mL
6	10000	10^4 cells/mL
7	100000	10^5 cells/mL
8	1000000	10^6 cells/mL

2.3 Data analysis

Experiment data records from the optical biosensor underwent processing through a MATLAB script which was built particularly for cell detection purposes. The MATLAB script

first organized reflection spectra into concentration categories after smoothing high-frequency noise using a low-pass filter. A peak and valley detection method based on prominence analysis extracted the local spectral features. Multiple trials of mean intensity measurements obtained at different concentration levels were used as the basis for analysis. Visual assessments from grouped spectral response data as mean intensity curves (corresponding to *b* and *c* for *Fig. 2, Fig. 4, and Fig.6*) and differential envelopes (corresponding to *d* and *e* for *Fig. 2, Fig. 4, and Fig.6*) allowed to study feature stability alongside concentration-related changes. The analysis separated peaks and valleys according to their locations in each spectral area to address possible asymmetries in optical elements. The wavelengths which exhibited the most consistent monotonic intensity variation were selected for sensitivity testing purposes. Sensor response tests utilized these trends for identifying detection methods that provided specific and repeatable cell identification.

Another MATLAB code served as a processor for spectral data obtained from cell detection experiments. The spectrum received initial partition into two sections due to eliminating transient filter effects while loading in data from the sensor's working spectral range. The minimum peak prominence threshold detected separate spectral peaks from baseline valleys throughout the analyzed spectrum. Each spectral feature identification led to an extraction of intensity values at each concentration level among the eight concentrations. Average intensity numbers based on repetitive test measurements across each concentration were computed before analyzing spectral trends to determine pure increasing or decreasing intensity patterns. The measured sensitivity of the assay comprised the complete range of intensity variation between minimum and maximum dB values. Features were selected from spectra because of their monotonic pattern then wavelength positions alongside sensitivity measurements were exported for analysis. The method helped to determine which wavelengths produced the most sensitive peak and valley responses to be used for cross-cell line comparisons.

CHAPTER 3 – RESULTS AND DISCUSSION

The nanoparticle doped optical fiber biosensors were designed for the detection of CD44 protein. These biosensors were likely to bring high biocompatibility, fast response and low cost to the table compared to other existing detection methods. The great potential offered by this biosensor to proceed to clinical trials lies in the process optimization of the fabrication, functionalization, and the detection processes, and to be co designed for additional cancer biomarkers in one device. The sensors were first fabricated by splicing SDI with SMF, reassuring a precise fusion with the loss in dB no more than 0.1 dB. Consequently, the fabricated sensors underwent the calibration stage. The sensor with sensitivities higher than 100 dB/mm were proceeded further for the functionalization. All sensors were introduced to the CD44 antibody binding. The performance of the optical biosensor was also assessed in terms of sensitivity and specificity using three different commercial human cell lines: HCC1806, MCF10A, and HEK293. Since the HCC1806 breast cancer cell line is a cell line that overexpresses the CD44 surface marker, it served as the primary target since this is relevant in cancer diagnosis. To assess the biosensor's specificity, malignant and normal breast tissue was distinguished using the MCF10A breast epithelial cell line. An additional negative control based on biologically unrelated cells was taken from HEK293 cells (human embryonic kidney tissue), which served in vitro as cells derived from another species than the healthy, breast cells used for control. Together these cells permitted the comparison of sensor behavior between cancerous, non cancerous, and tissue unrelated cells. MCF10A and HEK293 low signal responses, along with high signal response in HCC1806, would signify

the high selectivity of the sensor towards CD44 positive cancer cells and hence recruiting potential as a diagnostic sensor.

3.1 Biosensor calibration and HCC1806 cell line detection

HCC1806 cells are considered to show high proportion of the $CD44^{high}$ /$CD24^{low}$ phenotype, a marker associated with breast cancer stem cells (16). This phenotype contributes to the cells' stemness and tumorigenic potential. The detection of the SDI sensor bound to CD44 antibodies was expected to show high peak or valley response. *Fig. 2* demonstrates the calibration and detection results of the chosen sensor exposed to 8 different HCC1806 cell suspensions from. Concentration 1 refers to the PBS solution, while the consequent concentrations from 2 to 8, according to *Table 1*.

As expected, a strong signal response was observed across several spectral features, confirming the sensor's sensitivity toward CD44-positive cells, which is demonstrated in *Fig 2.* The calibrated sensor, the sensitivity of which was 132.7581 dB/RUI according to *Fig. 2a*, was functionalized and detected CD44 protein expression. *Fig. 2b* shows the average spectral intensity (dB) for peak values measured in the reflection spectrum for the eight concentration levels of the tested cell line. Sensitivity to the presence and amount of cells is represented by monotonic trend in signal with increasing. Identical to *Fig. 2b, Fig.2c* shows the values for the valleys, demonstrating some fluctuations. *Fig 2d* shows the differential intensity of spectral peaks and valleys across the full wavelength range of the sensor. The differential intensity is equivalent to the change in signal with respect to baseline or lowest concentration, including peak response and valley response. These show which spectral features respond

most to presence of cells. Differential values are higher in potential regions of sensor sensitivity, and higher values imply an optimal wavelengths to monitor sensor performance. The last subfigure, *Fig. 2e,* demonstrated the averaged differential envelopes of peaks and valleys.

Figure 2. Calibration and spectral response of the optical biosensor to varying PCC1806 cell concentrations. (a) Sensitivity of sensor to refractive index changes as a function of resonance wavelength. (b)Peak intensity trends across concentrations. (c) Valley intensity trends across concentrations. (d) Differential intensity envelope of peaks and valleys. (e) Averaged differential intensity envelope for identifying most responsive wavelengths

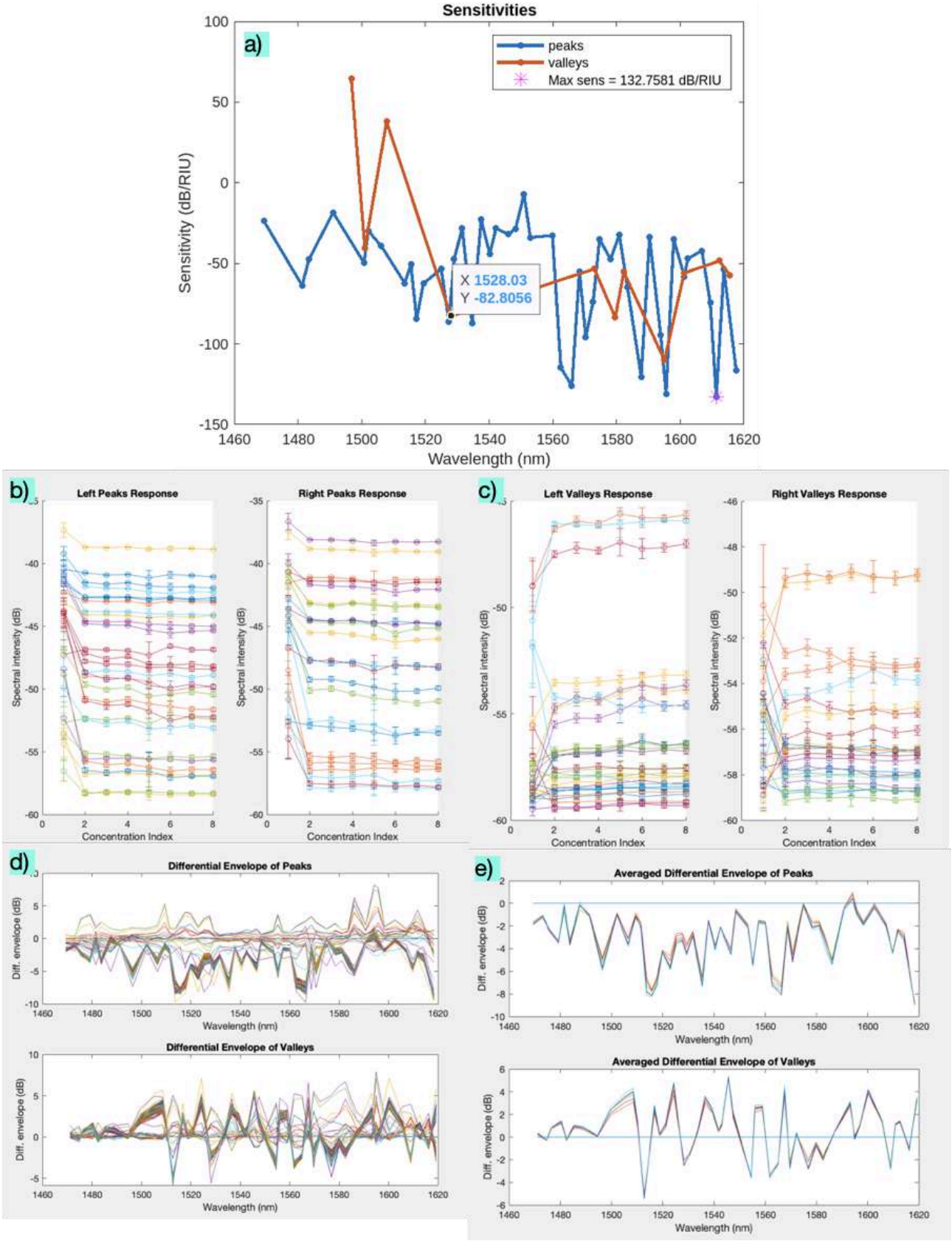

Further analysis took place to assess the sensitivity of the sensor, shown in *Fig. 3.* The detection sensitivity to HCC1806 cells achieved its highest value within the valley at

1544.416 nm because of stringent decreasing intensity patterns and a total 3.315 dB signal variation over the examined concentration range. The experiments confirm the research assumption since the HCC1806 cell line with well-documented CD44 overexpression interacts strongly with anti-CD44-functionalized sensors. The specific optical response pattern is strengthened by the dominant detection valley at high sensitivity together with its single localized detection range. The detecting capability of the sensor for CD44-expressing triple-negative breast cancer cells proves suitable through findings that support previous observations regarding optical biosensor detection of high CD44 expression.

Figure 3. Left spectrum intensity response curves across cell concentrations for HCC1806

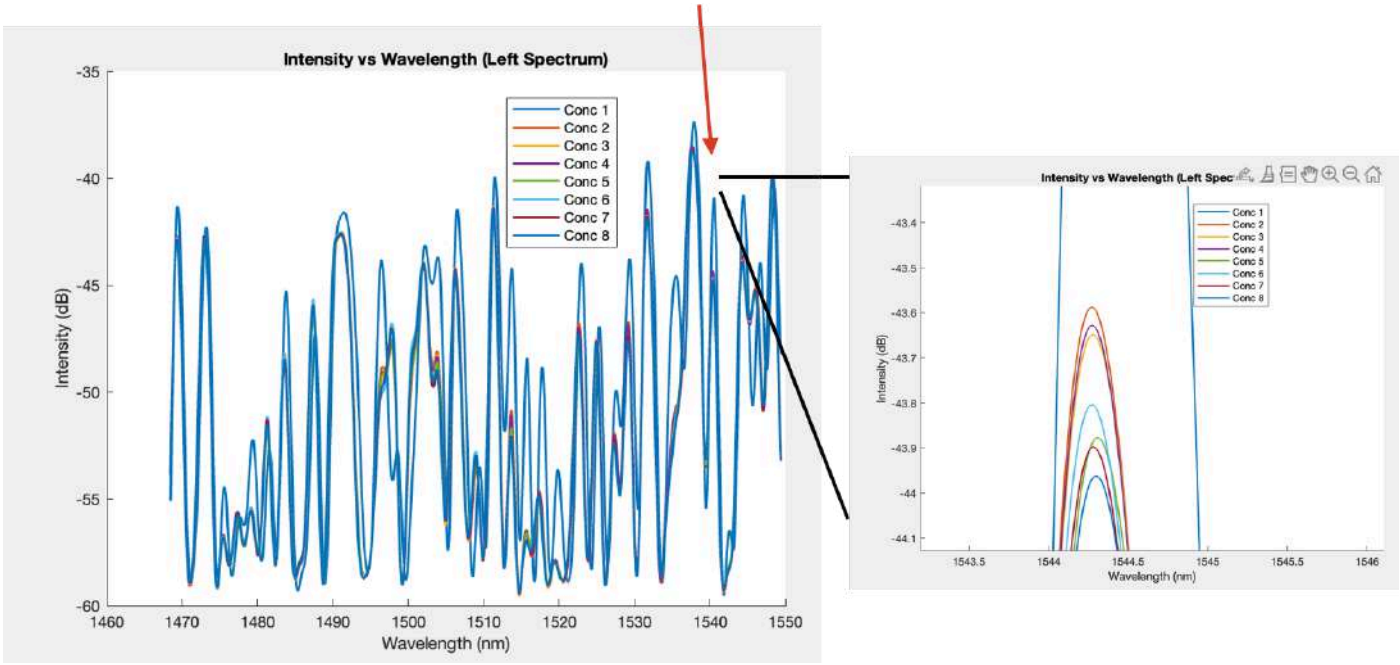

3.2 Biosensor calibration and MCF10a cell line detection

Although MCF10a cell line is a non-tumorigenic breast cancer epithelial cell line, it might express CD44 protein to some extent. The proportion of this population, however, highly depends on the factors such as the serum used for cell culture (17). Thus, while MCF10a cell line is generally considered to have low expression of CD44 proteins, it might still have $CD44^{+}$ phenotype, which was confirmed according to *Fig. 5*. This information was

taken into account during data interpretation. As a result of the calibration, the sensors with such sensitivities as 131.3959 dB/RUI were selected for functionalization and detection steps. *Fig. 4* demonstrates the calibration results of the sensor and the results of MCF10A cell line detection. *Fig. 4a* represents the sensitivity of one of such sensors after the calibration step. Following the next step, the sensor was introduced to PBS and seven MCF10A cell suspensions with varying concentrations, as shown in *Table 1* as well.

Figure 4. Calibration and spectral response of the optical biosensor to varying MCF10A cell concentrations. (a) Sensitivity of sensor to refractive index changes as a function of resonance wavelength. (b)Peak intensity trends across concentrations. (c) Valley intensity trends across concentrations. (d) Differential intensity envelope of peaks and valleys. (e) Averaged differential intensity envelope for identifying most responsive wavelengths

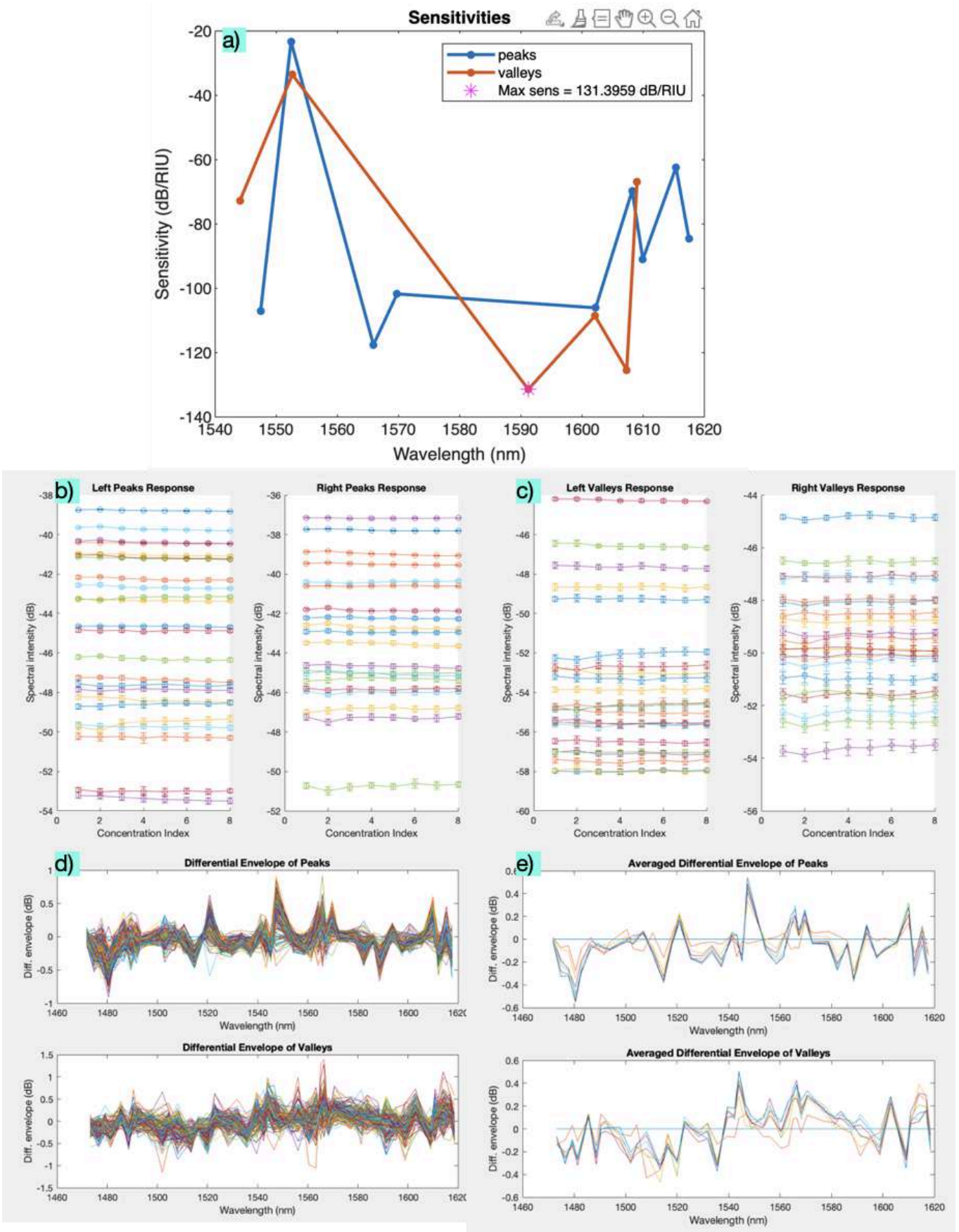
Sensitivities
a)
peaks
valleys
Max sens = 131.3959 dB/RIU
Sensitivity (dB/RIU)
Wavelength (nm)
b)
Left Peaks Response
Right Peaks Response
c)
Left Valleys Response
Right Valleys Response
Spectral intensity (dB)
Concentration Index
d)
Differential Envelope of Peaks
Differential Envelope of Valleys
e)
Averaged Differential Envelope of Peaks
Averaged Differential Envelope of Valleys
Diff. envelope (dB)
Wavelength (nm)

The MCF10A cells displayed decreased intensity at 1533.600 nm while the concentrations increased but did not show an increasing pattern at any wavelength, shown in *Fig.5.* The sensitivity measured at this wavelength was 0.110 dB. None of the spectral features presented either solely increasing or decreasing intensity patterns. The results suggest a limited and weak interaction between MCF10A cells and the surface of the functionalized sensor.

Figure 5. Left spectrum intensity response curves across cell concentrations for MCF10A

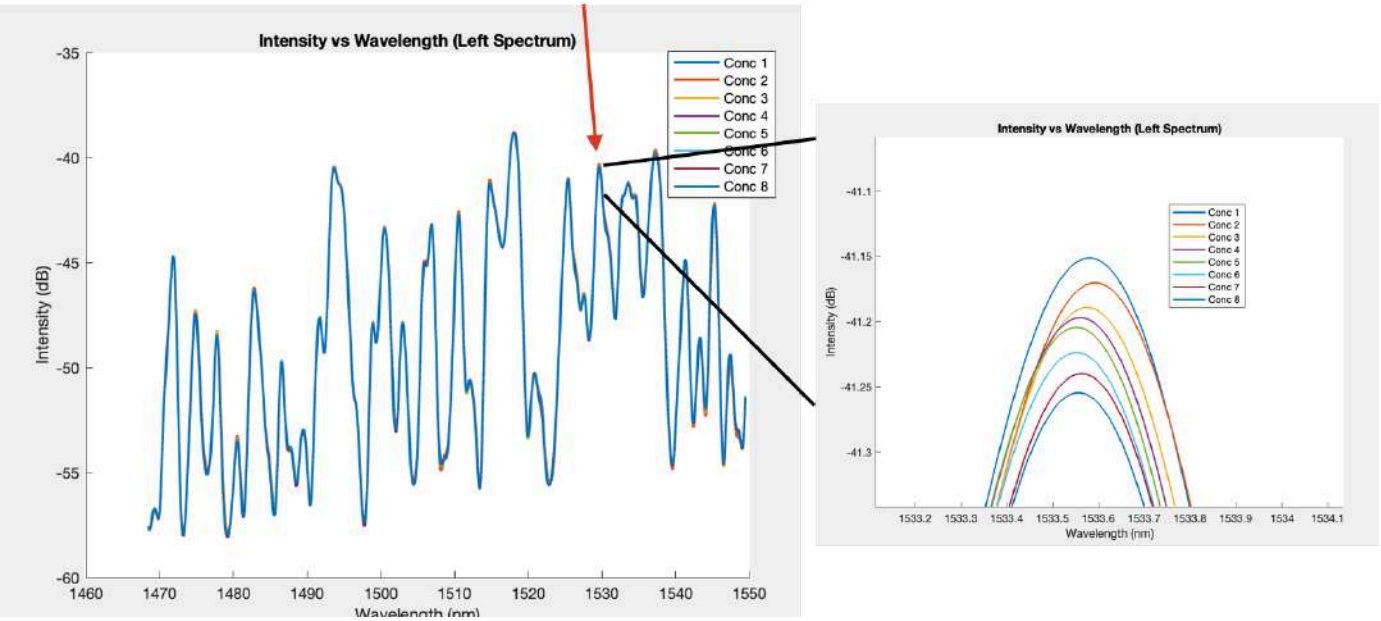

3.2 Biosensor calibration and HEK293 cell line detection

According to Birzele et. al., HEK293 cells do not naturally express CD44 (18). In their study, the researchers used wild-type HEK293 cells, which were CD44-negative and did not produce hyaluronic acid (HA). After transfecting with a CD44s expression vector, these cells began producing significant levels of HA and exhibited substantial transcriptional changes, indicating that CD44 expression was not present in the native HEK293 cells (18).

The HEK293 cell line delivered one of the most unexpected results during sensor detection evaluation, the results of which are shown in *Fig. 6.* The literature shows that regular HEK293 cells lack CD44 expression and perform as negative controls during CD44 research experiments (18). The detection results showed a reliable methodological response which spanned across each concentration point. The sensor demonstrated high sensitivity of 125.2308 dB/RIU through refractive index calibration before the HEK293 detection results could be processed, shown in *Fig. 6a.* Detections made across several wavelengths showed a progressive decrease in spectral intensity that was visible regardless of concentration rates in *Fig. 6b* and *6c*. The sensor surface interaction with cells produced an orderly decline in data which indicated the existence of quantifiable cellular reactions. *Fig. 6d* displayed a strong pattern regarding differential envelope responses which became evident in the valley locations. *Fig. 6e* demonstrates an averaged interpretation of that consistent pattern by identifying specific regions which showed uniform response throughout different concentrations.

Figure 6. Calibration and spectral response of the optical biosensor to varying HEK293 cell concentrations. (a) Sensitivity of sensor to refractive index changes as a function of resonance wavelength. (b)Peak intensity trends across concentrations. (c) Valley intensity trends across concentrations. (d) Differential intensity envelope of peaks and valleys. (e) Averaged differential intensity envelope for identifying most responsive wavelengths

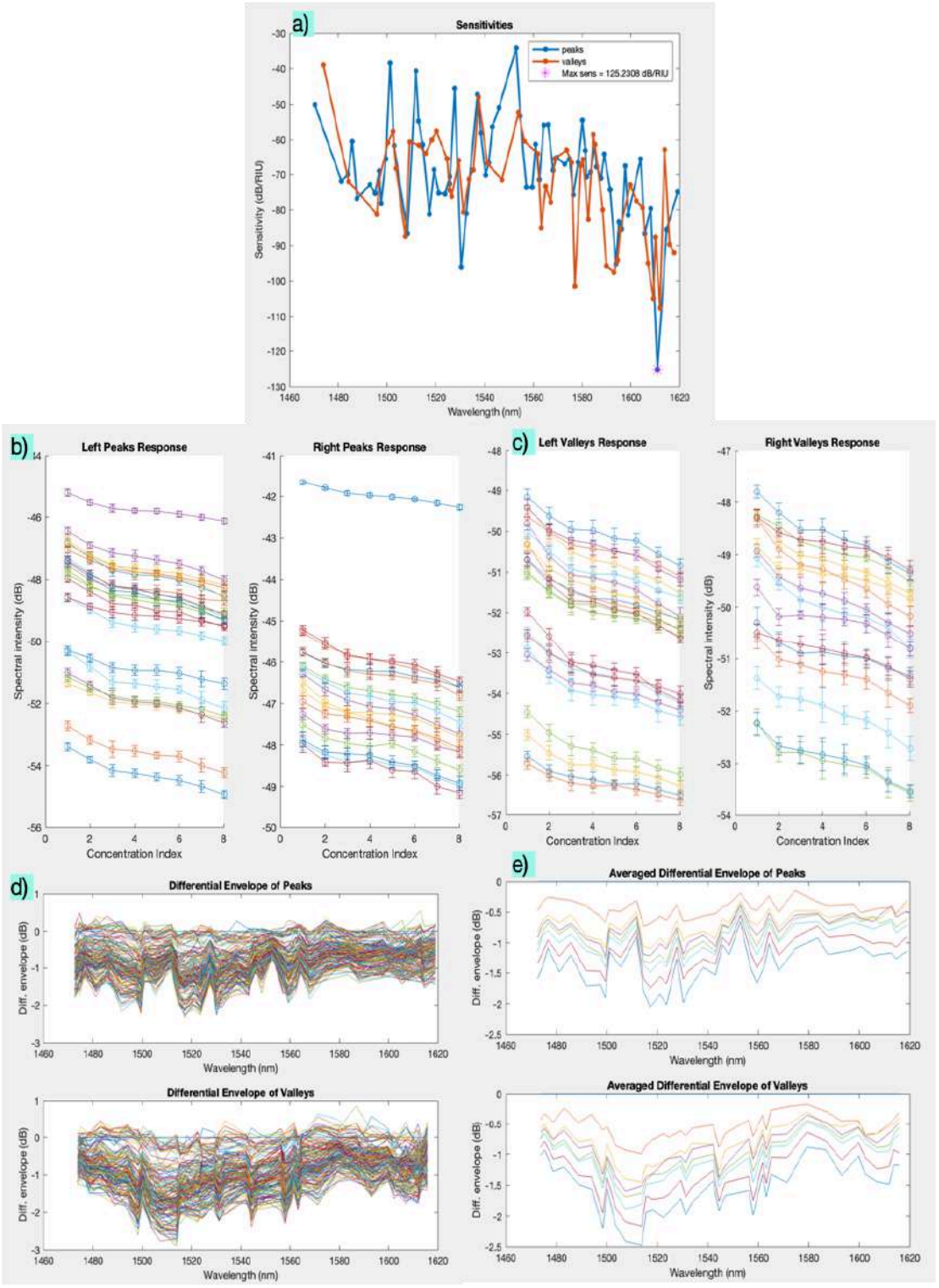

The presence of a clear and structured spectral response in HEK293 cells was also confirmed by 31 decreasing valleys and a strong signal at 1513.824 nm, shown in *Fig. 7.* This suggests the possibility of non-specific binding or CD44-independent interactions with the

sensor surface. Although the PEG-blocking took place and antibody-specific binding was used during functionalization, this significant finding in cellular absorption suggests that the CD44-negative cell line might exhibit either inadequate PEG blocking or non-specific protein interactions. Nevertheless, these findings emphasize the importance of using multiple control lines in biosensor development and highlight potential cross-reactivity in label-free systems.

The intensity pattern at a peak situated at 1513.824 nm decreased uniformly to indicate a sensitivity of 2.289 dB, which can be seen in *Fig. 7.*

Figure 7. Left spectrum intensity response curves across cell concentrations for HEK293

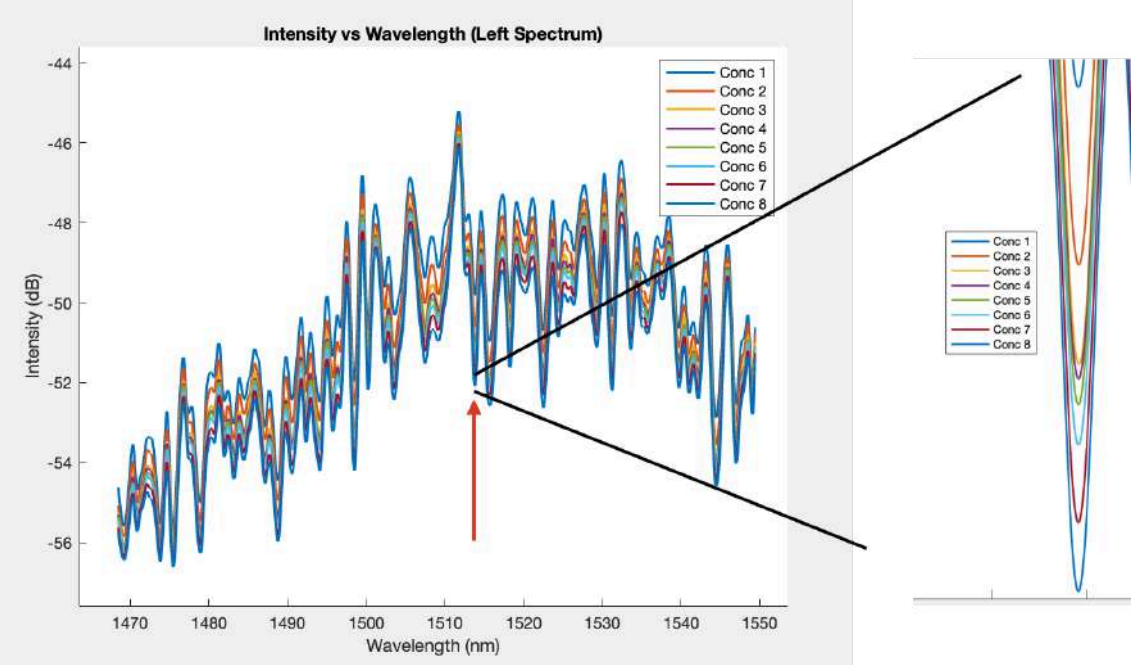

Several experiments are needed to understand the unexpected spectral results in HEK293 cells even though research shows these cells lack CD44 expression. The evaluation of surface CD44 expression should be done by running flow cytometry with anti-CD44 antibodies labeled with fluorescent markers to assess spontaneous changes in CD44 surface protein levels or those caused by cell cultivation. Western blot analyses and RT-PCR assessments should evaluate both CD44 protein quantities in addition to CD44 mRNA

abundance when confirming the molecular underpinning for such expression. The use of free anti-CD44 antibodies within a CD44-blocking assay before detection will help determine specific CD44-dependent binding if the sensor signal decreases. The definitive determination of CD44 as the binding factor requires controlled experiments by transfecting or knocking out CD44 in HEK293 cells or cells with changing CD44 expression. The distinction between specific binding and background interaction can be enhanced through additional experiments which involve testing alternative surface-blocking agents including BSA, Pluronic and longer PEG molecules. The supplementary experiments will identify actual HEK293 sensor reaction drivers and improve biosensor selectivity in forthcoming utilization.

The summarized results in *Table 2* demonstrate the differential response of the biosensor to each tested cell line.

Table 2. Summary of sensor response for three cell lines based on spectral feature analysis.

Cell Line	Feature type	Monotonic Trend	Wavelength (nm)	Sensitivity (dB)
HCC1806	Valley	Decreasing	1544.416	3.315
MCF10A	Valley	Decreasing	1533.600	0.110
HEK293	Valley	Decreasing	1513.824	2.289

For visual confirmation of the cells being attached to the surface of the sensor, it is also suggested to analyze the sensor's three different cell lines under SEM.

CHAPTER 4 – CONCLUSION

The thesis work focused on the development of a fiber optic biosensor system for CD44-expressing cell detection through using Micron Optics interrogator for spectral investigation. A biosensor was functionalized and bound to CD44 antibodies and PEG-based blocking agents to achieve selective binding together with non-specific interaction reduction. The measurements of sensor sensitivity using sucrose solutions resulted in such reported values as 132.7581 dB/RIU, 131.3959 dB/RIU, and 125.23 dB/RIU that verified the sensors' optical reaction ability before conducting cell detection. The biosensor detection tests involved three types of commercial human cells including HCC1806 (breast cancer) , MCF10A (breast epithelial), and HEK293 (embryonic kidney cells). The biosensor produced different detection signals that depended on the CD44 expression patterns of the analyzed cells. The HCC1806 cells, which are considered to be CD44-positive, produced the most impactful reaction through the 1544.416 nm light wavelength with a sensitivity value of 3.315 dB while confirming their CD44-positive characteristics. The MCF10A cellular signals remained minimal at just 0.110 dB indicating that the biosensor specifically selects malignant CD44-expressing cells, as it was generally expected. Although HEK293 cells were classified as CD44-negative, they showed a distinctive detection response at 1513.824 nm with a sensitivity measurement of 2.289 dB. The obtained results indicate a combination of non-specific binding and partial blocking effects together with low-level CD44-independent interactions which require further investigation. The research tests confirm that the biosensor operates as a label-free detection system that detects CD44-positive cells based on their concentration and exhibits strong potential for future diagnostic usage in cancer research.

Research data demonstrating clear distinctions between the sensor's reaction to HCC1806 and MCF10A cells confirms high sensitivity, while the results with HEK293 cell line suggests the need in further investigation and analysis, particularly, working on the specificity of the sensor. Further research should focus on identifying the sensor-cell reaction patterns through flow cytometry together with Western blotting assessment and CD44-blocking experiments along with better surface blocking approaches. Additionally, it is proposed to analyze the sensor surfaces under SEM after cell detection procedure. The diagnostic capabilities of this biosensor will benefit from additional testing with multiple cell lines and utilization of complex media to improve its functionality in actual patient scenarios. In the long run, designing optical fiber biosensor for breast cancer stem cell detection has promising perspectives, as they offer high sensitivity, ability to detect the cells remotely.

CHAPTER 5 – REFERENCES

[1]. Xu H, Niu M, Yuan X, Wu K, Liu A. CD44 as a tumor biomarker and therapeutic target. Exp Hematol Oncol. 2020 Dec 10;9(1):36. doi: 10.1186/s40164-020-00192-0. PMID: 33303029; PMCID: PMC7727191.

[2]. Sneath, R. J., and D. C. Mangham. “The normal structure and function of CD44 and its role in Neoplasia.” *Molecular Pathology*, vol. 51, no. 4, 1 Aug. 1998, pp. 191–200, https://doi.org/10.1136/mp.51.4.191.

[3]. Yaghobi Z, Movassaghpour A, Talebi M, Abdoli Shadbad M, Hajiasgharzadeh K, Pourvahdani S, Baradaran B. The role of CD44 in cancer chemoresistance: A concise review. Eur J Pharmacol. 2021 Jul 15;903:174147. doi: 10.1016/j.ejphar.2021.174147. Epub 2021 May 5. PMID: 33961871.

[4]. Ziranu P, Aimola V, Pretta A, Dubois M, Murru R, Liscia N, Cau F, Persano M, Deias G, Palmas E, Loi F, Migliari M, Pusceddu V, Puzzoni M, Lai E, Cascinu S, Faa G, Scartozzi M. New Horizons in Metastatic Colorectal Cancer: Prognostic Role of CD44 Expression. Cancers (Basel). 2023 Feb 14;15(4):1212. doi: 10.3390/cancers15041212. PMID: 36831554; PMCID: PMC9953769.

[5]. Chen, S., Zhang, S., Chen, S. *et al.* The prognostic value and immunological role of CD44 in pan-cancer study. *Sci Rep* 13, 7011 (2023). https://doi.org/10.1038/s41598-023-34154-3

[6]. Nolan E, Lindeman GJ, Visvader JE. Deciphering breast cancer: from biology to the clinic. Cell. 2023 Apr 13;186(8):1708-1728. doi: 10.1016/j.cell.2023.01.040. Epub 2023 Mar 16. PMID: 36931265.

[7]. Sung H, Ferlay J, Siegel RL, Laversanne M, Soerjomataram I, Jemal A, Bray F. Global Cancer Statistics 2020: GLOBOCAN Estimates of Incidence and Mortality Worldwide for 36 Cancers in 185 Countries. CA Cancer J Clin. 2021 May;71(3):209-249. doi: 10.3322/caac.21660. Epub 2021 Feb 4. PMID: 33538338.

[8]. McFarlane S, Coulter JA, Tibbits P, O'Grady A, McFarlane C, Montgomery N, Hill A, McCarthy HO, Young LS, Kay EW, Isacke CM, Waugh DJ. CD44 increases the efficiency of distant metastasis of breast cancer. Oncotarget. 2015 May 10;6(13):11465-76. doi: 10.18632/oncotarget.3410. PMID: 25888636; PMCID: PMC4484469.

[9]. Vadhan A, Hou MF, Vijayaraghavan P, Wu YC, Hu SC, Wang YM, Cheng TL, Wang YY, Yuan SF. CD44 Promotes Breast Cancer Metastasis through AKT-Mediated Downregulation of Nuclear FOXA2. Biomedicines. 2022 Oct 5;10(10):2488. doi: 10.3390/biomedicines10102488. PMID: 36289750; PMCID: PMC9599046.

[10]. Bekmurzayeva A, Ashikbayeva Z, Assylbekova N, Myrkhiyeva Z, Dauletova A, Ayupova T, Shaimerdenova M, Tosi D. Ultra-wide, attomolar-level limit detection of CD44 biomarker with a silanized optical fiber biosensor. Biosens Bioelectron. 2022 Jul 15;208:114217. doi: 10.1016/j.bios.2022.114217. Epub 2022 Mar 26. PMID: 35367702.

[11]. Kaur J, Srivastava R, Borse V. Recent advances in point-of-care diagnostics for oral cancer. Biosens Bioelectron. 2021 Apr 15;178:112995. doi: 10.1016/j.bios.2021.112995. Epub 2021 Jan 16. PMID: 33515983.

[12]. Ramirez-Valles EG, Rodríguez-Pulido A, Barraza-Salas M, Martínez-Velis I, Meneses-Morales I, Ayala-García VM, Alba-Fierro CA. A Quest for New Cancer Diagnosis, Prognosis and Prediction Biomarkers and Their Use in Biosensors Development. Technol Cancer Res Treat. 2020 Jan-Dec;19:1533033820957033. doi: 10.1177/1533033820957033. PMID: 33107395; PMCID: PMC7607814.

[13]. Lyu S, Wu Z, Shi X, Wu Q. Optical Fiber Biosensors for Protein Detection: A Review. *Photonics*. 2022; 9(12):987. https://doi.org/10.3390/photonics9120987

[14].Fujikura Europe Ltd. "News." *Fujikura Europe*, n.d., https://www.fujikura.co.uk/news.aspx?id=45. Accessed 9 Apr. 2025.

[15]. Lechuga, L. M., & Estevez, M. C. (2012). Integrated optical devices for lab-on-a-chip biosensing applications. *Laser & Photonics Reviews*, 6(4), 463–487. https://doi.org/10.1002/lpor.201100017

[16]. Guo, L., Ke, H., Zhang, H. *et al.* TDP43 promotes stemness of breast cancer stem cells through CD44 variant splicing isoforms. *Cell Death Dis* 13, 428 (2022). https://doi.org/10.1038/s41419-022-04867-w

[17]. Sheridan, C., Kishimoto, H., Fuchs, R.K. *et al.* CD44+/CD24-breast cancer cells exhibit enhanced invasive properties: an early step necessary for metastasis. *Breast Cancer Res* 8, R59 (2006). https://doi.org/10.1186/bcr1610

[18]. Birzele, Fabian, et al. "CD44 Isoform Status Predicts Response to Treatment with Anti-CD44 Antibody in Cancer Patients." *Clinical Cancer Research*, vol. 21, no. 12, 2015, pp. 2753–2762. https://doi.org/10.1158/1078-0432.CCR-14-2141.

APPENDICES

Appendix A

Figure A 1. The SEM image of the SDI sensor after the detection with MCF10A (no attached cells found)

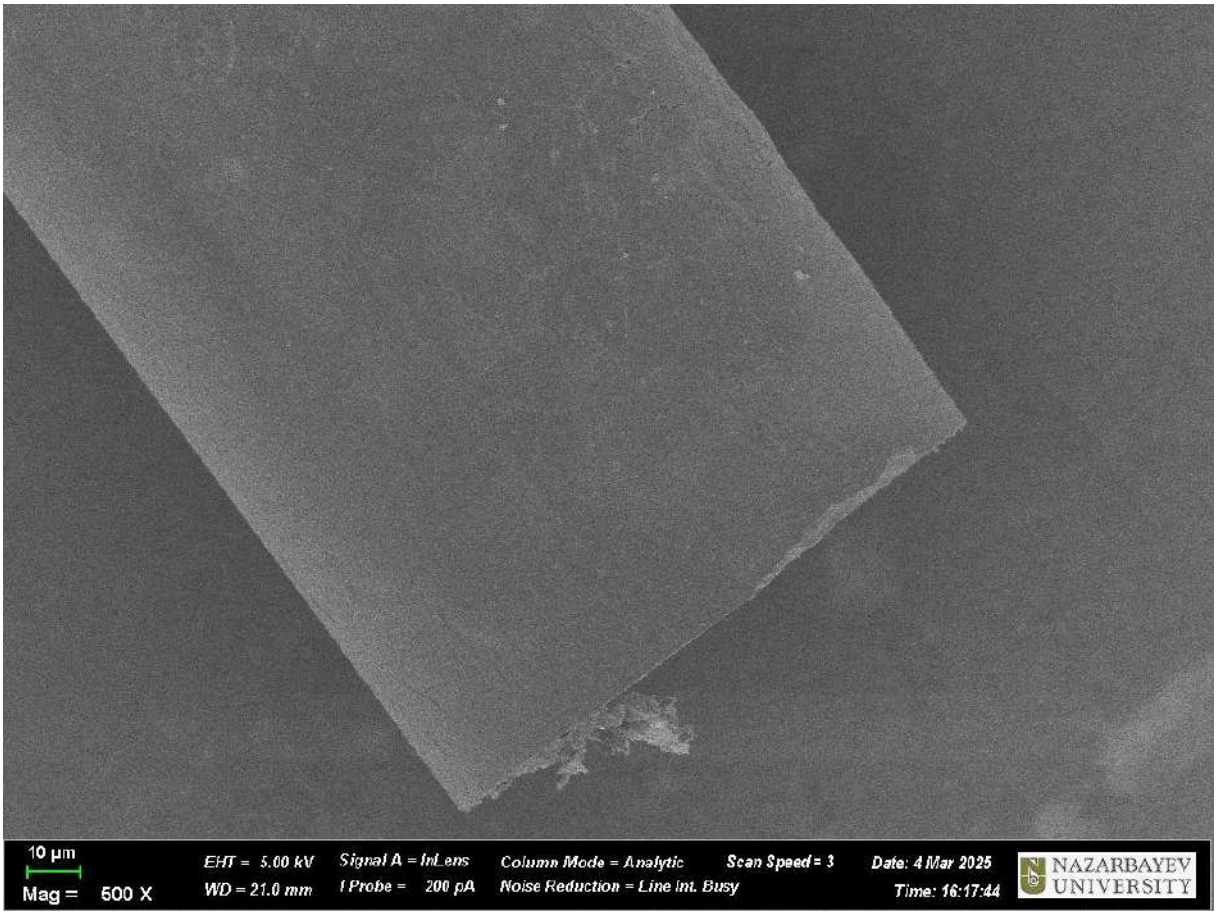

Appendix B

Figure B 1. Refractive Index Calibration Code Excerpt

```matlab
% Fit wavelength shift vs. RI to determine sensitivity
x = refractive_index_values;
y = corresponding_wavelengths;
p = polyfit(x, y, 1);       % Linear fit
sensitivity = p(1);         % Sensitivity in nm/RIU
R2 = rsquare(x, polyval(p,x)); % Goodness of fit
```

Figure B 2. Cell Detection Analysis Code Excerpt

```
% Apply low-pass filter and extract spectral peaks/valleys
filteredData = lowpass(ChannelData, 0.05);
[PksL, LocsL] = findpeaks(filteredData(1,1:split), 'MinPeakProminence', 1);
[ValsL, VLocsL] = findpeaks(-filteredData(1,1:split), 'MinPeakProminence', 1);

% Average spectral responses across concentrations
for i = 1:N_Conc
    start_idx = (i-1)*N_Val + 1;
    end_idx = i*N_Val;
    MeanSpectrum(i,:) = mean(filteredData(start_idx:end_idx,:), 1);
end
```

Figure B 3.Peak and Valley Detection Code Excerpt

```
% Identify peaks and valleys
[P, LocPeakLeft] = findpeaks(SpectrumLeft_P, 'MinPeakProminence', 1.5);
[P, LocValleyRight] = findpeaks(-SpectrumRight_P, 'MinPeakProminence', 1.5);

% Store intensity at each concentration
for i = 1:N_Conc
    start_idx = (i-1)*N_Val + 1;
    end_idx = start_idx + N_Val - 1;
    MeanSpectrumLeft(i, :) = mean(SpectrumLeft(start_idx:end_idx, :), 1);
end
```